

## Chemical microstructure of Franciscan jadeite from Pacheco Pass, California

MARTIN RADVANEC,<sup>1,\*</sup> SHOHEI BANNO,<sup>1</sup> AND W.G. ERNST<sup>2</sup>

<sup>1</sup>Department of Geology and Mineralogy, Kyoto University, Kyoto, 606-01, Japan

<sup>2</sup>Department of Geological and Environmental Sciences, Stanford University, Stanford, California 94305-2115, U.S.A.

### ABSTRACT

The chemical microstructure of five jadeitic pyroxenes from three Franciscan quartzose metagraywacke samples was investigated by backscattered electron imagery, element mapping, and electron microprobe microanalysis. These clinopyroxenes are neoblastic, subhedral grains or subradial aggregates replacing albite. For each compositionally zoned Cpx grain, a series of up to five parallel, polished sections were cut essentially normal or parallel to the crystallographic *c* axis. Five investigated grains, single and subradial aggregates, were examined quantitatively and three-dimensional chemical sections of the grains were constructed. Chemical zoning progresses from the Na-Cpx core to rim in four distinct regions (Q, L, Acm, and T). Region Q consists of microcrystalline blebs of quartz and jadeite ( $x_{jd} = 0.95$ ) and has a bulk composition of nearly pure albite. Very rarely it contains albite. L is jadeite ( $x_{jd} = 0.80$ ) that contains lawsonite inclusions. Acm is acmite-rich Cpx ( $x_{jd} = 0.65$ ), and T consists of TiO<sub>2</sub>-bearing jadeite (1–2 wt% TiO<sub>2</sub>,  $x_{jd} = 0.95$ ). Isolated Cpx grains and prismatic aggregates display the same chemical architecture regardless of crystallographic orientation. The earliest growth stage, Q, represents a volume-for-volume replacement of pre-existing albite by nearly stoichiometric jadeite plus quartz. As prisms grew, diffusion from the lithic matrix progressively enriched outer Na-Cpx zones in Fe<sup>3+</sup>, Ca, and Mg. Terminal stages of high-pressure growth are represented by TiO<sub>2</sub>-bearing jadeitic pyroxenes, possibly reflecting a temperature increase or relatively long-term annealing under the same conditions in the presence of titanite and rutile. The core Q and rim T regions represent a jadeite plus quartz assemblage and confirm our earlier notion that the jadeite zone of Franciscan metamorphic rocks was subducted to depths where the assemblage jadeite and quartz was stable, at pressures of more than 10 kbar.

### INTRODUCTION

Since recognition of the widespread occurrence of jadeitic pyroxene in Franciscan metagraywackes of the central Diablo Range, California Coast Ranges (McKee 1962), the Franciscan Complex has been regarded as a classic high-pressure (blueschist facies) metamorphic terrane. Ernst (1971) showed that in the Pacheco Pass area, where albite and jadeite occur together, neoblastic jadeite needles nucleated within precursor metastable albite, then grew as subhedral aggregates, and finally thoroughly replaced the pre-existing albite as coarse prisms. Maruyama et al. (1985) and Terabayashi et al. (1996) documented zoning in jadeitic pyroxene at Pacheco Pass and argued that jadeitic pyroxene crystallized under near-equilibrium conditions, coexisting stably with excess albite and quartz. These contrasting interpretations of the growth history of jadeitic pyroxene have led to different inferred *P-T* paths for the metamorphic complex and thus different tectonic interpretations of the subduction-zone metamorphic process.

Subradial fibrous-to-prismatic aggregates of jadeite that show wavy extinction are an important metamorphic phase in Franciscan graywackes (Bloxam 1956). The chemical structure of this mineral is most clearly revealed by backscattered electron images (BEI) combined with quantitative electron microprobe analysis. This technique was used by Brothers and Grapes (1989) to support their much-contested hypothesis for the detrital origin of the jadeite grains. On the basis of a more recent BEI study, Ernst and Banno (1991) proposed that, at Pacheco Pass, jadeite-bearing metagraywackes overstepped the univariant *P-T* equilibrium curve defined by the assemblage of pure jadeite + quartz + albite and entered the *P-T* stability field of jadeite + quartz, where nearly pure jadeitic pyroxene crystallized irreversibly. This inferred crystallization history is consistent with the earlier interpretation of Ernst (1971). All recent studies have documented the heterogeneity of Na-clinopyroxene (Na-Cpx) in the Pacheco Pass metamorphic graywackes, where jadeite contents in zoned grains range between  $x_{jd} = 0.65$  and 0.95.

The present study quantifies the detailed chemical microstructure of Franciscan jadeitic pyroxene to further constrain the growth mechanism of this high-pressure

\* On leave from Geological Survey of Slovakia, 05240, Spis-ska Nova Ves Slovakia.

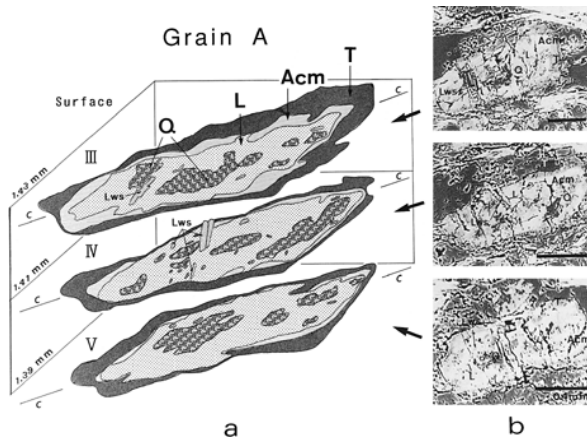


**FIGURE 1.** Grain A (sample SB770312F), these sections are approximately (010) with the *c* axis inclined about 5° obliquely. Interval 0.02 mm arc. (a) Sketch. (b) BEI. Numbers on the left side show the height of polished surfaces III, IV, and V. Sketches are based on BEI and element mapping for Ca, Al, Si, Fe, and Ti, and 27 spot analysis. Q = jadeite + quartz; L = jadeitic pyroxene + minor lawsonite; Acm = acmitic jadeite; T = Ti-bearing jadeite; Lws = lawsonite.

phase. We constructed three-dimensional images of Na-Cpx chemistry to obtain insights into the kinetics of crystallization and the tectonic history of the metamorphic complex. Earlier petrographic work (Ernst 1971, 1993; Maruyama et al. 1985; Ernst and Banno 1991) documented stages in the progressive replacement of detrital albite by jadeitic pyroxene: (1) fibrous needles and aggregates are enclosed in the plagioclase; (2) individual grains lengthened parallel to the *c* axis but also substantially enlarged normal to the *c* axis, (3) growth continued to ultimately result in stubby prismatic pyroxene.

We examined five jadeitic pyroxenes in three metagraywackes from the Pacheco Pass area of the Diablo Range; locations of the rock samples and constituent mineral assemblages are presented in the appendix. A Hitachi electron microprobe equipped with a Kevex analytical system, Kevex 8000 and Quantum detector (energy dispersive), was used throughout this study, following the method described by Mori and Kanehira (1984) and Hirajima and Banno (1991). Pyroxene nomenclature follows Morimoto (1988). Polished surfaces are optically flat except for some grain boundary and the tips of crystal aggregates. Appropriate grains were selected according to their morphology as observed by backscattered electron image.

#### CHEMICAL MICROSTRUCTURE OF JADEITIC PYROXENE

##### Sample SB770312F2

A slab 1.55 mm thick was prepared from this metagraywacke specimen. The polished and carbon-coated surface I was examined by electron microprobe; then the slab was thinned approximately 0.02 mm as measured by

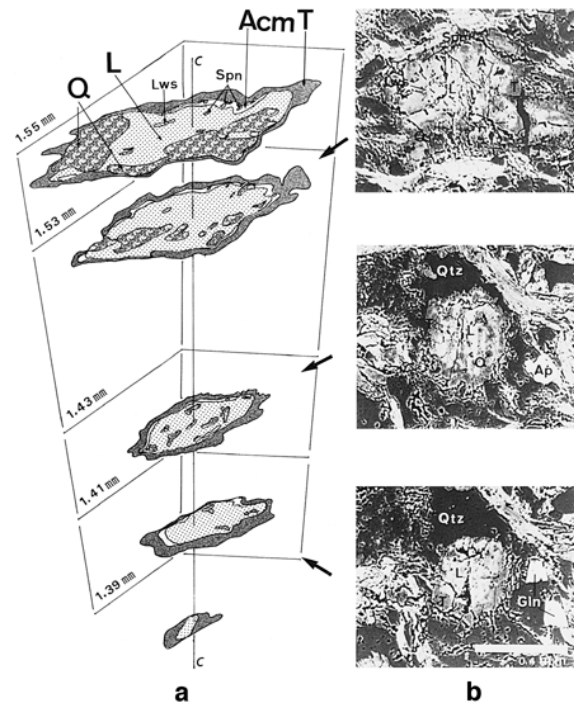


**FIGURE 2.** Grain B (sample SB770312F), subnormal to the *c* axis. (a) Sketch. (b) BEI. Spn = titanite; Ap = apatite; Gln = glaucophane. These are matrix minerals. Other symbols are the same as in Figure 1.

screw micrometer, and a new surface II (1.53 mm) was polished, carbon-coated, and examined by electron microprobe. This procedure was repeated, and surfaces III (1.43 mm), IV (1.41 mm), and V (1.39 mm) were examined sequentially. Grain A, a single grain elongated subparallel to the *c* axis, which was studied in greatest detail, appeared on polished surfaces III, IV, and V (see drawings and BEIs in Fig. 1). After the electron microprobe study, polished surface V was adhered to a glass slide, the original slide was removed, then the slab was reduced to 0.03 mm thickness for microscopic examination. Grain B appeared in all five polished surfaces. The *c* axis of grain B (see drawings and BEIs in Fig. 2) lies subnormal to the slab as estimated from traces of two cleavages at nearly 90°. These cleavage traces appeared on all five surfaces, but grain B was almost completely lost on polished surface V; thus an adequate photomicrograph could not be prepared. A composite grain, C (composed of one crystal subparallel to and another subnormal to the *c* axis; pictures not shown here) was studied on two surfaces. The two surfaces of grain C possess a chemical structure similar to that of grains A and B. All three analyzed Cpx grains consist of four regions with distinct chemical and mineralogical characteristics. These regions are designated Q, L, Acm, and T, corresponding to quartz-bearing, lawsonite-bearing, acmite-rich, and Ti-rich regions, respectively. Twenty-seven quantitative spot analyses were performed to better characterize the chem-

**TABLE 1.** Representative analyses of jadeitic pyroxene

Grain Region	Single grain (SB770312F)					Radial aggregate (WGE-38)			WGE-47 E T
	A Q	A L <sub>min</sub>	A L <sub>max</sub>	A Acm	A T	D Q	D L	D Acm	
SiO <sub>2</sub>	58.96	56.84	57.46	56.49	59.09	59.34	58.95	57.05	59.76
TiO <sub>2</sub>	0.18	0.02	0.07	0.04	1.75	0.04	0.07	0.06	1.45
Al <sub>2</sub> O <sub>3</sub>	22.47	19.58	18.11	15.43	22.25	22.76	21.49	17.56	21.41
FeO*	3.05	5.54	6.85	9.92	1.15	1.90	3.28	7.13	2.94
MnO	0.05	0.08	0.08	0.11	0.05	0.06	0.13	0.12	0.07
MgO	0.49	0.28	0.65	0.90	0.34	0.35	0.49	0.54	0.30
CaO	0.50	2.00	1.75	2.12	0.09	0.61	1.18	1.57	0.29
Na <sub>2</sub> O	15.33	12.88	13.66	13.29	15.20	14.71	14.58	13.42	14.98
Total	101.03	97.22	98.63	98.30	99.92	99.77	100.17	97.44	101.20
Si	1.99	2.02	2.01	2.01	2.00	2.01	2.01	2.02	2.01
Ti	0.00	0.00	0.00	0.00	0.04	0.00	0.00	0.00	0.04
Al	0.89	0.82	0.75	0.65	0.89	0.91	0.86	0.73	0.85
Fe <sup>3+</sup>	0.09	0.07	0.18	0.27	0.04	0.05	0.09	0.19	0.08
Fe <sup>2+</sup>	0	0.10	0.02	0.02	0	0	0	0.02	0.00
Mn	0.002	0.002	0.002	0.005	0.001	0.002	0.004	0.004	0.002
Mg	0.02	0.01	0.03	0.05	0.02	0.02	0.02	0.03	0.02
Ca	0.02	0.08	0.07	0.08	0.00	0.02	0.04	0.06	0.01
Na	1.0	0.89	0.93	0.92	1.00	0.97	0.96	0.92	0.98
Σ	4.01	3.99	3.99	4.00	3.99	3.98	3.98	3.97	3.99
Na + Ca	1.02	0.96	1.00	1.00	0.99	0.99	1.00	0.98	0.99
Si*	1.98	2.03	2.02	2.01	2.00	2.02	2.01	2.03	2.02

Notes: See text for ferrous and ferric determinations. L<sub>min</sub> and L<sub>max</sub> denote the most Jd-poor and -rich analyses.

\* Si is atomic content of Si when Σ(cation) = 4.

ical regions in the pyroxenes in this sample. Representative chemical compositions of jadeitic pyroxene in each region are listed in Table 1. The compositions of associated minerals and a broad beam (20 μm) chemical analysis of region Q are presented in Table 2.

For the pyroxene analysis, the Fe<sub>2</sub>O<sub>3</sub> content was estimated as Fe<sup>3+</sup> = Na - Al - Ti (or Fe<sup>3+</sup> = total Fe if Na - Al ≥ total Fe). The total number of cations and the sum Na + Ca justifies this procedure. All cations sum to

about 4 and Si is slightly (0.01 on average) higher than 2.0 (Table 1). The Si contents, based on total cation = 4, are also shown for reference. The small systematic errors of the analyses do not affect our petrological discussion. Complete tables of the analyses may be requested from the senior author (M.R.). Compositional ranges of pyroxenes from various regions of this pyroxene are shown in Figure 3.

The compositions of the pyroxenes in regions L and

**TABLE 2.** Analysis of associated minerals in SB770312F2

Mineral	Lawsonite	Phengite	Glaucofanone	Region Q
Occurrence	Inclusion in Jd	Matrix	Matrix	Replacement of Ab
SiO <sub>2</sub>	39.31	53.64	56.48	68.26
TiO <sub>2</sub>		0.11	0.13	0.04
Al <sub>2</sub> O <sub>3</sub>	32.14	22.53	10.72	16.96
FeO (total Fe)	0.30	4.13	18.80	2.96*
MnO	0.06	0.09	0.33	0.11
MgO		3.58	3.90	
CaO	17.11		0.06	0.42
Na <sub>2</sub> O	(0.15)†	0.12	7.42	11.79
K <sub>2</sub> O		9.55		
Total	88.92	93.75	97.84	100.54
Si	2.050	3.636	8.058	3.016
Ti		0.005	0.013	0.001
Al	1.986	1.800	1.802	0.878
Fe (total)	0.014	0.234	2.243	0.109
Mn	0.00	0.002	0.020	0.002
Mg	0.00	0.356	0.820	0.0020
Ca	0.974	0.00	0.010	0.020
Na		0.016	2.052	1.012
K		0.825	0.073	
Number of O atoms	9	11	23	8

\* Contamination from neighboring jadeite.

† Adjusted for chemical formula.

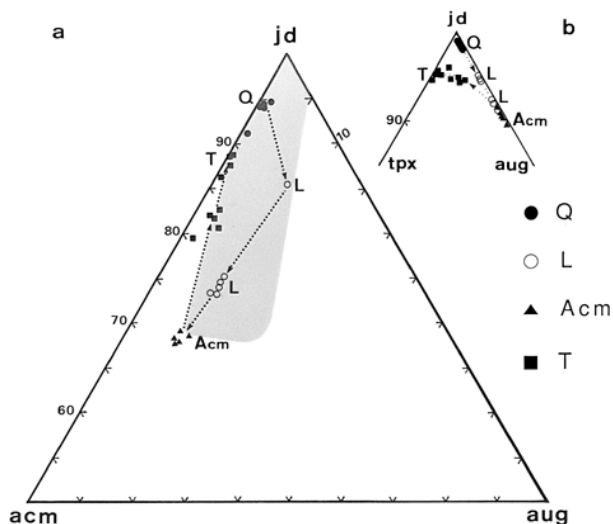


**FIGURE 3.** Compositional diagrams of pyroxenes of grain A. (a) jd (jadeite): acm (acmite): aug (augite) ratios. (b) jd: aug: tpx (Ti-Cpx). Gray area is the compositional area of Terabayashi et al. (1996, Fig. 10).

Acm are similar to those reported by Maruyama et al. (1985) and Terabayashi et al. (1996; see Fig. 3), but these authors did not recognize this peculiar Ti-bearing jadeite. However, Brothers and Grapes (1989, see their Fig. 5F) and Grapes (1992, see his Fig. 2) reported similar chemical ranges, including TiO<sub>2</sub>-rich (1.8–2.5 wt%) jadeite. Figure 4 presents a BEI of region Q, which is a mixture of jadeite with  $x_{jd} = 0.95$  and tiny quartz inclusions (2–5  $\mu\text{m}$  in diameter). Because region Q is extremely fine-grained, the optical continuity of jadeite in that region could not be evaluated. The overall broad-beam analysis of region Q is close to that of albite except for significant Fe content reflecting the presence of an acmite component in jadeitic pyroxene (Table 2). We do not understand why the Fe concentration in region Q is higher than that expected based on the mode of jadeitic pyroxene + quartz. In region Q of grain A (Fig. 1), we detected fine-grained, pure albite, presumably a relic of precursor albite. Region L, containing Cpx + Lws, consists mostly of jadeite accompanied by fine needles (<1 mm in length) of lawsonite. On BEIs, lawsonite and acmite-bearing Na-Cpx zones are not easily distinguished, but these regions are readily identified on element maps of Ca. In region L,  $x_{jd} = 0.75\text{--}0.85$  and  $x_{acm} = 0.23\text{--}0.13$ . In region Ac, Na-Cpx is acmitic jadeite with  $x_{jd} \approx 0.65$  and  $x_{acm} \approx 0.35$  and is typically accompanied by fine-grained titanite (1–3  $\mu\text{m}$ ). Region T is composed solely of TiO<sub>2</sub>-rich jadeite, with  $x_{jd} = 0.90\text{--}0.95$  and TiO<sub>2</sub> = 1–2 wt%. No titanite is included in this pyroxene.

A combination of Figures 1, 2, and 4 provides insight regarding the three-dimensional microchemical structure of the neoblastic pyroxene. Region Q consists of polygonal islands of intimately intergrown microcrystalline quartz and relatively pure jadeite. Regions L and Ac

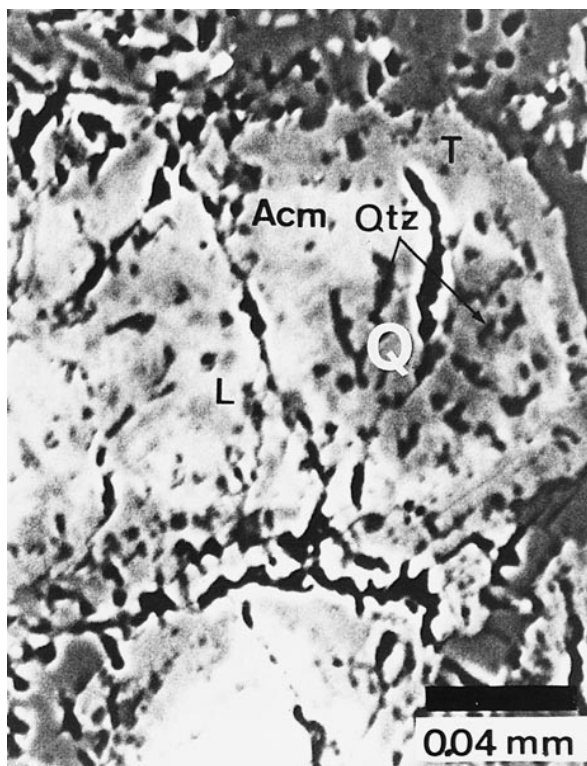


**FIGURE 4.** BEI of region Q of grain A. Dark polygonal area on the right-hand side of the figure consists of gray jadeite and black quartz.

become progressively more acmite-rich regions of prismatic jadeite. A discontinuity separates the outer part of region Ac from the encircling rim of region T. The manner in which the jadeitic pyroxene grew may be seen in Figures 1 and 2. Albite was first replaced by an aggregate of jadeite + quartz, which was then partly replaced and overgrown by a single jadeitic pyroxene crystal, whose acmite content increases toward the rim. Grain B (Fig. 2) also displays discontinuous armoring of regions Q by region L, which in turn is progressively armored by region Ac. The outermost region, T, discontinuously encircles region Ac.

#### Sample WGE-38

Figure 5 shows BEIs of a subradial aggregate of jadeitic pyroxene, grain D, elongated subparallel to the *c* axis. Table 1 lists the chemical compositions of various parts of this subradial aggregate. Letters on Figures 5a and 5b indicate the chemical regions determined by electron microprobe spot analyses. This pyroxene has five regions: Q, L, Ac, T, and I (I = interstitial), respectively. Region I consists of jadeitic pyroxene that developed as fine bands (1–4 mm) elongated parallel to the *c* axis. Region I is too thin for quantitative analyses but electron microprobe analyses of the area covering region I and surrounding region Ac yield compositions 2 wt% lower FeO (total Fe) than the average of the region L, and it is

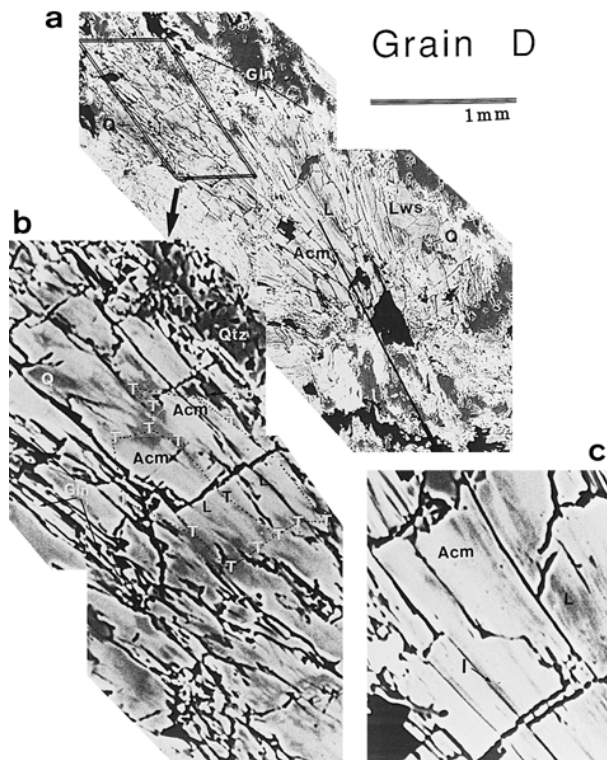


**FIGURE 5.** Grain D (sample WGE-38), subradial aggregate, nearly (010) with the  $c$  axis inclined about  $5^\circ$ . I = interstitial jadeite. Other symbols are the same as for Figures 2 and 3.

darker in BEIs (lower in mean atomic number) than region T. This observation suggests that region I is richer in jadeite than region L and poorer in  $\text{TiO}_2$  than region T. Figure 5c exhibits a complicated mixture of regions L and AcM in the center of the radial aggregate. Note that the contrast of these BEIs have been adjusted to detect region I, hence regions L and AcM are not clearly separated. In Figure 5, the radial aggregate appears to be composed of prisms (rectangles in the figure) elongated parallel to the  $c$  axis. Region I represents either a late precipitate along the boundary of these rectangles or portion of growth zoning. We prefer the first interpretation because the textural features illustrated by Ernst (1992, his Fig. 2), who presented a BEI of jadeitic pyroxene that projects into a quartz vein, showed that prismatic growth domain is clearly defined and bordered by a compositional region comparable to I. Near the tip of the aggregate in Figure 5b, the enlargement of the tip of the subradial aggregate, the boundaries of the rectangles are occupied locally by glaucophane (Gln) and titanite. Region I is not recognized here.

#### Sample WGE-47

The sketch in Figure 6a illustrates the chemical structure of a typical subradial aggregate based on the findings shown in Figure 5. Figure 6b shows the BEI image of another aggregate, grain E in sample WGE-47, cut sub-

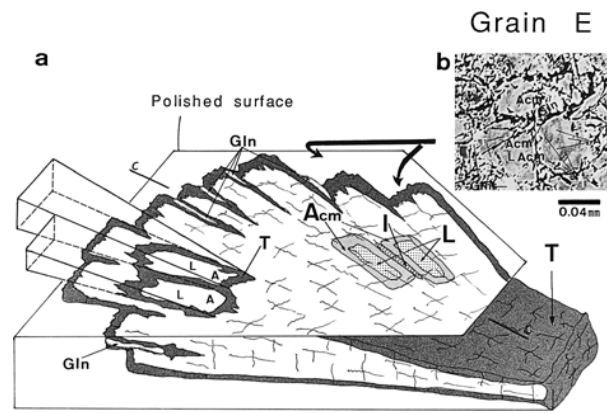


**FIGURE 6.** (a) Schematic diagram showing the chemical structure of subradial aggregate. It consists of a bundle of growth prisms. The central portion of the picture shows why the growth unit is rectangle on a section cut subparallel to the  $c$  axis. (b) BEI of grain E (sample WGE-47), cut normal to the  $c$  axis. Arrow shows the direction of Figure 6b. The upper plane is a polished surface.

normal to the  $c$  axis. This sample shows chemical and textural features similar to those in sample WGE-38 described above. Both metagraywackes contain subradial aggregates of jadeitic pyroxene with remnant albite and matrix lawsonite, quartz, and glaucophane. The pyroxene illustrated in Figure 6b (sample WGE-47) possesses the same chemical structure as the pyroxene analyzed in WGE-38. In Figure 6b, ellipsoidal regions composed of regions L and AcM are surrounded by region T, indicating that the rectangles detected in Figure 5 (parallel to the  $c$  axis) are likely lengthwise cross sections of prisms. The fact that this sample, WGE-47, (Fig. 6b) contains Ti-rich jadeite (T) and glaucophane (Gln) suggests that this is a section cut subnormal to the  $c$  axis, near the tip of the subradial aggregate. Thus, the complicated region T in Figures 5b and 5c is interpreted as the traces of prisms on slightly oblique sections.

## DISCUSSION

### Proposed model for growth of subradial aggregates

The growth history of single grains of jadeitic pyroxene is simple, as briefly described for sample SB770312F2 (see Fig. 6). For a subradial aggregate of pyroxene, we interpret that the point of origin for the subradial prismatic aggregate was at the lower right of the Figure 6a, and that growth proceeded to the upper-left of the figure. Slightly wedge-shaped prisms tended to widen with growth. Misfits between the prisms were filled by region I. Each prism developed by crystallizing region Q and is zoned with region L covering region Q, which in turn is covered successively by region AcM and then region T. Regions L and AcM grew subsequently as the results of reaction between nearly pure jadeite developed by the decomposition of albite and multi-component pore solution associated with the host metagraywacke. This

implies that the material migrated easily along the boundaries of prisms. Region T represents the latest precipitate not only in our study of jadeitic pyroxenes but also in Pacheco Pass textures illustrated by Brothers and Grapes (1989, their Fig. 5E) and Grapes (1992, his Fig. 2c). The texture of jadeitic pyroxene described here is not consistent with the detrital jadeite hypothesis of Brothers and Grapes (1989). Pyroxene clasts in sandstone should have been abraded, resulting in disruption of the systematic core-to-rim chemical systematics.

#### Formation of zonal structure

Two explanations have been proposed for the texture of jadeitic pyroxene of Franciscan metagraywackes from the Pacheco Pass area. Maruyama et al. (1985) and Terabayashi et al. (1996) recognized complex zoning in jadeitic pyroxene, and attributed the chemical heterogeneity of jadeitic pyroxene to small fluctuations of physical conditions (40–50 °C) during growth. Using the compositions of jadeitic pyroxene for geothermobarometry and assuming that equilibrium was attained among jadeitic pyroxene, quartz, albite, and other coexisting minerals, they concluded that the *P-T* path of Franciscan graywackes did not cross the univariant line of jadeite + quartz = albite reaction. Their *P-T* path is convex toward the univariant line and touches but does not cross it. Ernst (1971) claimed that in most cases precursor albite coexisted metastably with neoblastic jadeite plus quartz. Based on their BEI textural study, Ernst and Banno (1991) suggested that the Franciscan jadeitic pyroxene did not exhibit growth zoning controlled by surface equilibrium accompanied by changing physical conditions. They proposed instead that the observed heterogeneity was due to irreversible crystallization of clinopyroxene in the *P-T* stability field of pure jadeite plus quartz. Our new results demonstrate that jadeitic pyroxene is systematically zoned, more regularly than considered previously (e.g., Ernst and Banno 1991). However the shapes of isochemical surfaces revealed in sections normal to the *c* axis (Figs. 2, 6b) demonstrate that the isochemical surface is irregular and does not appear to be the growth surface of near-equilibrium crystallization. If so, we expect a subhedral texture, as seen in augite in ordinary metabasites. Instead, the presence of such an internal structure supports irreversible crystallization proposed by Ernst and Banno (1991).

The process that formed region Q of the zoned jadeitic pyroxene is related to the overall process of replacement of clastic albite by neoblastic pyroxene. The jadeite in region Q approaches end-member, with  $x_{jd} = 0.95$  and  $x_{acm} = 0.05$ , and differs in composition from that of pyroxene expected in equilibrated metagraywackes that contain appreciable amounts of Fe<sub>2</sub>O<sub>3</sub>, CaO, MgO, etc. The formation of region Q demonstrates clearly that the graywackes entered the *P-T* stability field of jadeite + quartz. Following initial growth, the composition of the neoblastic pyroxene replacing albite evolved toward that of the equilibrium pyroxene, an acmite-rich jadeitic py-

roxene of region Acm. This resulted in the formation of chemical zoning from the regions L to Acm. This proposed growth history contrasts with the case where a mineral of low intracrystalline diffusion rate grows maintaining surficial equilibrium at all times with all coexisting phases. If this latter process, generalized as being a Rayleigh fractionation process, had operated, region Acm should have occurred at the core, armoured successively by zones of progressively more jadeite-rich pyroxene. This expected result for Rayleigh fractionation conflicts with the observed textural and chemical relationships.

The significance of region T as representing the last stage of crystallization is still not well understood. These zones have replaced regions of Acm pyroxene that contained titanite inclusions, which subsequently were dissolved in region T jadeite by a temperature increase or long-term annealing. Or, it may be that, near the terminal stages of growth, the matrix supplying “impurities” was exhausted of sufficiently mobile cations, with only titanium contributing to the composition of the enlarging nearly stoichiometric NaAlSi<sub>2</sub>O<sub>6</sub>. A rim of Ti-rich jadeite is certainly common to all of the samples studied thus far but future work should attempt to determine the distribution of such pyroxene across a metamorphic field gradient to evaluate these hypotheses.

#### Implications for metamorphic *P-T* path

A remaining crucial question concerns whether or not the chemical structure records the changing physical conditions during growth of the pyroxene. The formation of region Q, consisting of nearly pure jadeite + quartz, demonstrates the entry of detrital albite into the *P-T* stability field of stoichiometric jadeite + quartz. The formation of fine-grained mineral aggregates such as these contrasts with the expectation for near-equilibrium metamorphic crystallization and suggests possible rapid crystallization. Perhaps as a result of the irreversible replacement of albite during overstepping of the univariant curve of albite = jadeite + quartz reaction. This view is supported by the fact that region Q exists both in matrix albite-bearing (subradial, WGE-38) and matrix albite-free (single grain, SB770312F12) metagraywackes. It demonstrates that the difference in mineral mode of these metagraywackes corresponds to the extent of (mineralogical) change (see Prigogine and Defay 1954) but not to differences in physical conditions. The Ti-rich jadeite rims show that the metagraywackes were in the jadeite + quartz *P-T* field at the terminal stage of metamorphic reaction. Therefore we envisage that most of pyroxenes were formed under similar physical conditions. If  $x_{jd}$  is taken as a *P-T* indicator, as assumed by Maruyama et al. (1985) and Terabayashi et al. (1996), the zoning could be interpreted as having been initiated by irreversible recrystallization of albite to jadeite + quartz. Decreasing pressure or increasing temperature of crystallization would have produced pyroxenes of regions L and Acm, finally returning to the jadeite + quartz field with forming of Ti-bearing jadeite at the rim. This process is not consistent with the *P-T* path proposed

by Maruyama et al. (1988) and Terabayashi et al. (1996) that did not enter the jadeite-quartz field. Furthermore the process involved is one of pyroxene decomposition and an albite-forming reaction, except for in region T, and such zoning should be associated with resorption of jadeitic pyroxene. We observed no new albite grown in place of jadeitic pyroxene, except for late neoblastic albite in extensional cracks of jadeite and a single possible example of a jadeite decomposition texture presented by Grapes (1992, his Fig. 3A). If jadeite decomposed to albite, we need to assume that the coexisting albite is not detrital but a decomposition product of jadeite, an idea no one has yet proposed. On the other hand, in our model the source of jadeite component is in region Q and the neoblastic Na-Cpx more-or-less replaced albite (not volume for volume except for region Q); the compositional change is mainly due to the exchange of Al of the region Q jadeite and Fe<sup>3+</sup> in the environment. The apparently metastable coexistence of quartz + albite + jadeitic pyroxene is observed not only under the microscope, but also at the scale of the electron microprobe as shown by Ernst and Banno (1991, Fig. 2) and in region Q of Figure 4.

Regarding the *P-T* path of the jadeitic pyroxene-bearing metagraywacke in the Pacheco Pass area, we reaffirm our earlier conclusion (Ernst 1988; Ernst and Banno 1991) and emphasize that Franciscan rocks passed into the *P-T* stability field of stoichiometric jadeite + quartz during prograde metamorphism. The temperature apparently did not exceed 300 °C, because of the preservation of aragonite (Carlson and Rosenfeld 1981; Hacker et al. 1992).

It follows that the exhumation of the Franciscan Complex immediately followed subduction and that the compression and decompression *P-T* paths did not differ significantly. The subduction complex did not remain at depth long enough to be warmed appreciably by heat transfer. The *P-T* path of Ernst (1988) supported by this study, implies that the model invoking deceleration of the down-going slab by subduction of seamounts (Maruyama and Liou 1989) requires further substantiation. We emphasize that additional detailed mineralogical and petrological work is necessary to further elucidate the tectonic history of this metamorphic complex.

#### ACKNOWLEDGMENTS

The Japanese Association for Promotion of Science (JSPS) provided long-range and short-period fellowships to M.R. and W.G.E., respectively. T. Hirajima helped to operate the electron microprobe, H. Tsutsumi and K. Irino enthusiastically and meticulously prepared thin sections and photographs. M. Kitamura, I. Sunagawa, C. Jacobson, G. Harwell, J. Gooch, T. Rushmer, and G. Bebout critically but constructively reviewed the manuscript. Our hearty thanks to these people for their support.

#### REFERENCES CITED

- Bloxam, T.W. (1956) Jadeite-bearing metagraywackes in California. *American Journal of Science*, 41, 488–496.
- Brothers, R.N. and Grapes, R.H. (1989) Clastic lawsonite, glaucophane and jadeitic pyroxene in Franciscan metagraywackes from the Diablo Range, California. *Geological Society of America, Bulletin*, 101, 14–26.
- Carlson, W.R. and Rosenfeld, J.L. (1981) Optical determination of topotactic aragonite-calcite growth kinetics: metamorphic implications. *Journal of Geology*, 89, 615–638.
- Ernst, W.G. (1971) Petrological reconnaissance of Franciscan metagraywackes from the Diablo Range. *Journal of Petrology*, 12, 413–437.
- (1988) Tectonic history of subduction zones from retrograde blueschist *P-T* paths. *Geology*, 16, 1081–1084.
- (1992) Neoblastic jadeitic pyroxene in Franciscan metagraywacke from Pacheco Pass, central Diablo Range, California, and implication for the inferred metamorphic *P-T* path. Reply. *New Zealand Journal of Geology and Geophysics*, 35, 385–387.
- (1993) Geology of the Pacheco Pass Quadrangle, central California Coast Ranges. *Geological Society of America, Map and Chart Series MCH078*, 1:24,000.
- Ernst, W.G. and Banno, S. (1991) Neoblastic jadeitic pyroxene in Franciscan metagraywacke from Pacheco Pass, central Diablo Range, California and implication for the inferred metamorphic *P-T* trajectory. *New Zealand Journal of Geology and Geophysics*, 34, 285–292.
- Grapes, R.N. (1992) Neoblastic jadeitic pyroxene in Franciscan metagraywacke from Pacheco Pass, central Diablo Range, California, and implications for the inferred metamorphic *P-T* trajectory: Comment. *New Zealand Journal of Geology and Geophysics*, 35, 381–387.
- Hacker, B.R., Kirby, S.H., and Bohlen, S.R. (1992) Time and metamorphic petrology. *Science*, 258, 110–113.
- Hirajima, T. and Banno, S. (1991) Electron-microprobe analysis of rock-forming minerals with Kevex Delta IVB (Quantum detector). *Hitachi Science Instruments News*, 56, 37–46 (in Japanese with English abstract)
- Maruyama, S. and Liou, J.G. (1989) Possible depth limit of underplating by seamount. *Tectonophysics*, 160, 327–337.
- Maruyama, S., Liou, J.G., and Sasakura, Y. (1985) Low temperature recrystallization of Franciscan graywackes from Pacheco Pass, California. *Mineralogical Magazine*, 49, 345–335.
- McKee, B. (1962) Widespread occurrence of jadeite, lawsonite and glaucophane in central California. *American Journal of Science*, 260, 596–610.
- Mori, T. and Kanehira, K. (1984) X-ray energy spectrometry for electron probe analysis. *Journal of Geological Society of Japan*, 90, 271–285.
- Morimoto, N. (1988) Nomenclature of pyroxenes. *American Mineralogist*, 73, 1123–1133.
- Prigogine, I. and Defay, R. (1954) *Chemical Thermodynamics*. Wiley, New York.
- Terabayashi, M., Maruyama, S., and Liou, J.G. (1996) Thermobarometric structure of the Franciscan complex in the Pacheco Pass region, Diablo Range, California. *Journal of Geology*, 104, 617–636.

MANUSCRIPT RECEIVED DECEMBER 2, 1996

MANUSCRIPT ACCEPTED OCTOBER 20, 1997

#### APPENDIX

Localities and mineral assemblages of studies specimens:

**SB770312F.** Collected directly west of Pacheco Pass. Slightly foliated. Major constituents are Cpx, quartz, lawsonite, glaucophane, and hematite. Small amounts of a mixture of native cooper-zinc and rutile armored by titanite are present. Albite occurs only in region Q as relics.

**WGE-38.** Collected 1 km east of Pacheco Pass (see Ernst 1993). Consists of quartz, albite, subradial aggregate of jadeitic pyroxene, lawsonite, titanite, phengite, chlorite, and glaucophane.

**WGE-47.** Collected 2 km south of Pacheco Pass (see Ernst 1993). Quartz, albite, subradial aggregates of jadeitic pyroxene, carbonate, titanite, lawsonite, phengite, chlorite, and glaucophane are major constituents.